JOURNAL OF GEOPHYSICAL RESEARCH, VOL. 102, NO. C7, PAGES 15,647–15,657, JULY 15, 1997

Simulations of the Atlantic Ocean with a free surface sigma coordinate ocean model

Tal Ezer and George L. Mellor
Program in Atmospheric and Oceanic Sciences, Princeton University, Princeton, New Jersey

Abstract. A sigma coordinate, free surface numerical model with turbulence dynamics has been implemented for the Atlantic Ocean and the Greenland Sea, from 80°S to 80°N. It is driven at the surface by monthly mean sea surface temperature and wind stress climatologies and is executed for 30 years. This is the first time that a model of this type, previously used mostly for coastal and regional simulations, has been implemented for the entire Atlantic Ocean and run for a long period of time. The model horizontal circulation, thermohaline overturning circulation, and meridional heat fluxes are described; the results are compared with observations and the results of other models. The model produces intense deep western boundary currents and complicated gyre structures associated with small-scale topographic variations. The meridional overturning circulation consists of about 14 Sv (1 Sv = 10^6 m^3 s^{-1}) of southward flowing deep water mass crossing the equator and a northward heat flux with a maximum value of more than 1 PW (10^{15} W). Although the maximum meridional heat flux is comparable to estimates obtained from observations, the amplitude of the seasonal variations of northward heat flux across 26°N is underestimated in comparison with observations; it is similar to that obtained by other models.

1. Introduction

The Atlantic Ocean and its interaction with the Greenland-Iceland and Norwegian (GIN) seas, where a large portion of the world ocean's deep water formation occurs, have been the focus of extensive observational and numerical studies aimed at understanding climate change. Numerical ocean models and coupled ocean-atmosphere models [e.g., *Delworth et al.*, 1993], developed in recent years, are the major tools used to study interannual and interdecadal climate variabilities. Most of the previous numerical simulations of the Atlantic Ocean used models based on the Bryan-Cox model developed at the Geophysical Fluid Dynamics Laboratory and known as the Modular Ocean Model (MOM) [*Pacanowski et al.*, 1991]; in particular, the Community Modeling Effort (the CME model) is described by *Bryan and Holland* [1989] and *Bryan et al.* [1995]. Isopycnal ocean models have also been used for large-scale simulations of the Atlantic Ocean [*Oberhuber*, 1993; *New et al.*, 1995]. A recent study [*Chassignet et al.*, 1996] compared the two types of models and shows that there are considerable similarities between results obtained by a z level model, which uses the eddy-induced isopycnal mixing parameterization of *Gent and McWilliams* [1990], and results obtained by an isopycnal coordinate model; both models have more realistic meridional overturning and heat fluxes than a z level model with a standard horizontal mixing; a similar conclusion has been also presented by *Böning et al.* [1995].

Another type of model, used here, is the free surface, bottom-following sigma coordinate Princeton Ocean Model (POM) [*Blumberg and Mellor*, 1987; *Mellor*, 1996], which has a turbulence submodel for surface and bottom mixed layer dynamics. This model has been originally developed for estuarine and coastal studies and only recently has been applied to basin-scale and climate problems [*Häkkinen and Mellor*, 1992; *Ezer and Mellor*, 1994; *Ezer et al.*, 1995; *Mellor and Ezer*, 1995]. However, this is the first time that decadal-long simulations have been executed with this type of model for a basin-scale domain such as the entire Atlantic Ocean. Therefore it is useful to compare differences and similarities between the general circulation of this model and those of other models mentioned above, even though no attempt has been made to use identical configurations and surface forcing. Such comparisons are to be found in other studies, which focus on large-scale processes [*Gerdes*, 1993], Gulf Stream dynamics [*Willems et al.*, 1994], and coastal processes [*Haidvogel and Beckman*, 1997]. One finding of these and other studies is that a sigma coordinate ocean model is attractive for simulating processes associated with bottom topography such as flow over sills, continental shelf flows, tidal flows, and bottom boundary layers dynamics; thus sigma layer models have been widely used in studies of coastal regions. Because of the way bottom topography is treated in a bottom-following vertical coordinate system, the barotropic flow associated with the bottom slope is well represented in the model even in the limit of one layer. By comparison, a sloping bottom in a z level model cannot be modeled with one layer, and multiple layers produce a step-like structure that may not accurately represent bottom boundary layer flows. The effect of bottom topography in large-scale ocean circulation models is important, since the circulation is largely driven by the joint effect of baroclinicity and bottom relief (JEBAR), as shown, for example, by the diagnostic models of *Mellor et al.* [1982], *Greatbatch et al.* [1991], and *Ezer and Mellor* [1994]. Furthermore, *Myers et al.* [1996] and *Dengg et al.* [1996] suggest that misrepresentation of this term in ocean models may be responsible for the unrealistic Gulf Stream separation in Atlantic Ocean models.

Paper number 97JC00984.
0148-0227/97/97JC-00984$09.00

An issue that has been of some concern in atmospheric and ocean sigma coordinate models is an identifiable error in the calculation of horizontal pressure gradient (PG) terms on a sigma coordinate grid over steep topography [*Haney*, 1991]. *Mellor et al.* [1994] have analyzed this error for the particular numerical scheme used by POM and have shown the following: (1) The scheme is convergent, so the PG error decreases with the square of the vertical and horizontal grid size, even when the so-called hydrostatic inconsistency condition [see *Haney*, 1991] is violated. (2) A test of a two-dimensional channel flow with steep side walls shows that the PG error is reduced to an insignificant level after integrations of the order of months. (3) In a three-dimensional model with realistic topography, some residual error remains; smoothing of topographic features with the largest slopes and subtracting the area averaged climatological density field before calculating PG terms reduce errors to values that are small in comparison with the mean flow and other numerical errors. The above procedure has been followed here and in most previous applications of sigma coordinate models. Comparing the standard sigma coordinate PG calculation with a calculation in which the PG term is calculated on z levels (and all other terms are calculated the same way as in the sigma model), *Mellor et al.* [1994], with a coarse resolution North Atlantic model, demonstrated that there are no significant errors in surface elevation or stream function as long as the standard procedure of bottom smoothing and removing the area-averaged density field from the PG calculations is done.

This paper is organized as follows: First, in section 2, the model and its setting for the Atlantic domain are described, then, in section 3, different aspects of the model climate and circulation features are presented, and finally, discussion and conclusions are offered in section 4.

2. Model Setting

The primitive equation Princeton Ocean Model, described by *Blumberg and Mellor* [1987] and *Mellor* [1996], has a free surface, bottom-following vertical sigma coordinate and a turbulence sub-model [*Mellor and Yamada*, 1982]. The Atlantic model grid and bottom topography are shown in Figure 1. The resolution of the curvilinear orthogonal horizontal grid varies between $\Delta x \approx 20$ km near the Antarctic Circumpolar Current (ACC) region ($\Delta y > \Delta x$ there) to $\Delta x \approx \Delta y \approx 50$ km in the Gulf Stream region and $\Delta x \approx \Delta y \approx 100$ km elsewhere. The sigma coordinate has 16 vertical layers, σ = (0.0, -0.0017, -0.0035, -0.0069, -0.0139, -0.0278, -0.0556, -0.1111, -0.2222, -0.3333, -0.4444, -0.5555, -0.6666, -0.7777, -0.8888, -1.0) and $\sigma = (z-\eta)/(H+\eta)$, where $\eta(x,y)$ and $H(x,y)$ are the surface elevation and water depth, respectively. The vertical resolution is higher near the surface and lower near the bottom (for example, for a grid point where water depth is 3000 m, Δz is about 5 m at the surface and about 300 m near the bottom). The horizontal time differencing is explicit, whereas the vertical differencing is implicit. The latter eliminates time constraints for the vertical grid and permits the use of fine vertical resolution near the surface and in shallow regions. At stable thermocline depths the turbulence closure submodel yields vanishingly small values of vertical viscosity and diffusivity to which is added, however, a constant background value of 2×10^{-5} m^2 s^{-1}. The model has a split time step: a two-dimensional external mode that uses a short time step of 44 s and a three-dimensional internal mode time step of 2000 s. The model grid extends from the deep ocean to 10 m depth on the continental

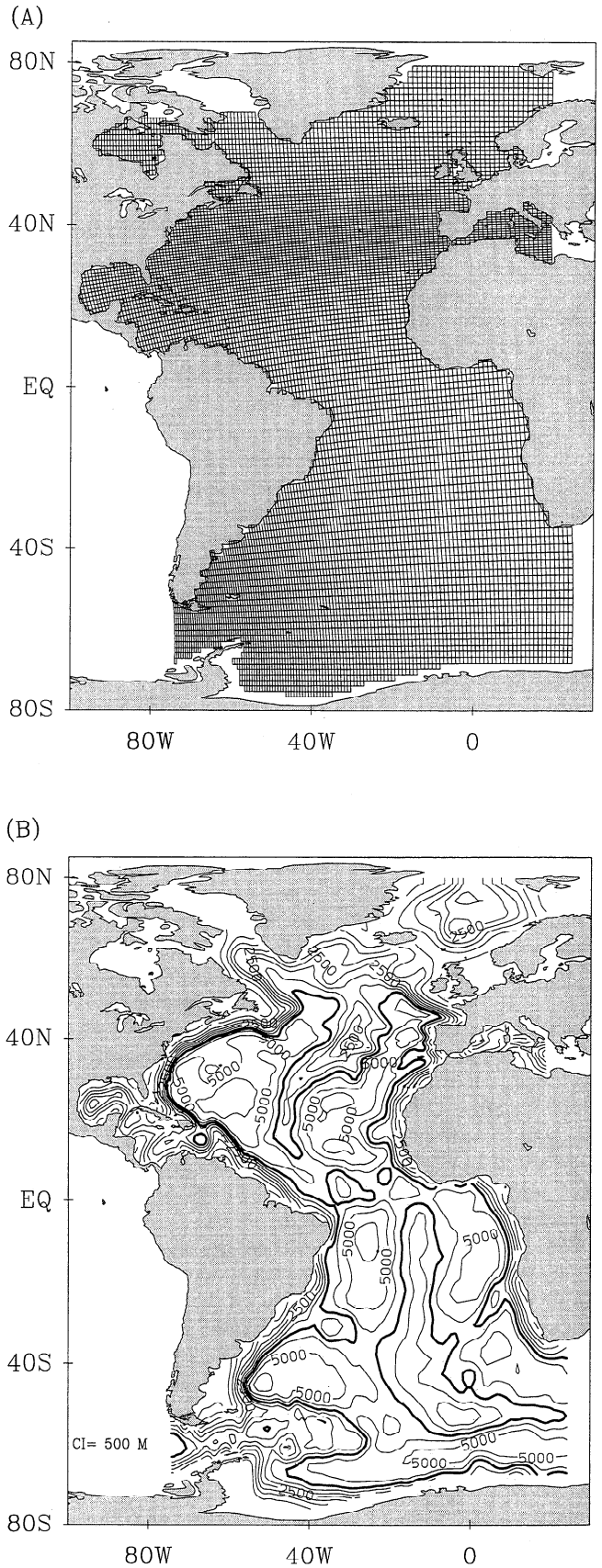

Figure 1. (a) Model grid and (b) bottom topography. The minimum depth of the coastal boundary is 10 m; the contour interval in Figure 1b is 500 m with a bold line indicating the 4000 m contour.

shelf, so that shallow regions such as the Hudson Bay are included in the calculations. The maximum bottom slope allowed between two adjacent grid points is $\Delta H/H < 0.4$; this, in addition to a Laplacian smoother is sufficient to eliminate significant pressure gradient errors as discussed above. The western Mediterranean is also included in the model domain (with a closed eastern boundary) and is connected to the North Atlantic with one grid cell representing the Gibraltar straits. Therefore the flow through the straits is controlled by the model dynamics without constraint except for the surface temperature boundary conditions in the western Mediterranean. The recent study of *Hecht et al.* [1997] indicates that model-simulated thermohaline circulation of the North Atlantic may be sensitive to changes in Mediterranean outflow on timescales of 100 years or more; for our relatively short integrtation period, changes of this type should not be important. At the three open boundaries (one in the north and two in the south), vertically averaged inflow/outflow are prescribed on the basis of observations and models, while for the baroclinic velocities, Sommerfeld-type radiation conditions are used. The *Levitus* [1982] annual climatology of temperature and salinity are prescribed on the open boundaries. Upwind advection boundary conditions allow the advection of the climatological temperatures and salinities into the model domain under inflow conditions. This type of boundary condition has been used successfully in previous applications of POM [*Ezer and Mellor*, 1992, 1994; *Ezer et al.*, 1995]. At the Fram Strait in the north, 5 Sv (1 Sv = 10^6 m^3 s^{-1}) total inflow and 5 Sv total outflow are prescribed along the western and eastern sides of the strait, respectively; the barotropic transport is distributed along the boundary according to the Arctic model of *Häkkinen and Mellor* [1992]. In the south, 135 Sv total inflow and outflow of the ACC, similar to the observed transport [*Whitworth and Peterson*, 1985], is prescribed at the western and eastern boundaries; the barotropic transport is distributed along the boundary according to the diagnostic models of *Mellor et al.* [1982] and *Fujio et al.* [1992].

The model is initialized with the annual *Levitus* [1982] climatology and then run for 30 years. Surface forcing includes the Levitus monthly climatological sea surface temperature and monthly climatological wind stress obtained from the Comprehensive Ocean-Atmosphere Data Set (COADS) analyzed by *da Silva et al.* [1994]. The data analysis includes climatological data obtained from the monthly mean values calculated from data collected over the period 1945 to 1989 and monthly anomalies for each month during this period.

The monthly SST data are used as the surface boundary condition for the turbulence model [*Mellor and Yamada*, 1982], which then can distribute the changes in SST downward and produce the seasonal change in the mixed layer temperature and depth. Experience with the MOM code also indicates that such a strong surface constraint is better suited for use with the *Mellor and Yamada* [1982] scheme than with the simpler convective adjustment scheme; the latter may result in very noisy heat fluxes and other numerical problems (R. Pacanowski and A. Rosati, personal communication, 1996). A common approach is to relax the model temperature to the observed SST within the first few layers by using a relaxation timescale that can range between a few days and a few months. However, *Tziperman et al.* [1994] and others have shown that simulated ocean variability is significantly affected by the choice of the relaxation timescale. Variations in freshwater fluxes also may be an important source of interannual variations in thermohaline circulation, as is indicated by many studies [*Weaver et al.*, 1991; *Tziperman et al.*, 1994; *Greatbatch et al.*, 1995]. However, here surface salinities are held fixed at the annual mean but spatially variable values. As expected, the surface conditions for temperature and salinity resulted in very small interannual variations when climatological mean surface values are used; this finding is actually useful in our particular sensitivity studies, since it will allow us to later remove model climate drift when variabilities associated solely with changes in surface forcing are studied.

As demonstrated, for example, by *Böning et al.* [1995], simulations of the thermohaline circulation may be quite sensitive to the formulation of horizontal diffusion in ocean models. A Smagorinsky-type horizontal diffusion is used here [*Smagorinsky et al.*, 1965] such that the diffusion coefficient is calculated according to

$$A_M = C\,\Delta x\,\Delta y\left[\left(\frac{\partial u}{\partial x}\right)^2+\frac{1}{2}\left(\frac{\partial v}{\partial x}+\frac{\partial u}{\partial y}\right)^2+\left(\frac{\partial v}{\partial y}\right)^2\right]^{1/2}$$

where u and v are the horizontal velocity components and C is a coefficient taken here as 0.2. In early versions of POM the diffusion terms were transformed so that the diffusion was effectively horizontal, the same as z level models. However, *Mellor and Blumberg* [1985] found that the component of horizontal diffusion normal to a sloping bottom produced unrealistic bottom boundary layer behavior, presumably a problem also indigenous to z level models. Thus, in the above and in most applications of sigma coordinate ocean models, diffusion of momentum and scalar fields are formulated along sigma surfaces incorporating the correct physics of bottom boundary layer dynamics, which dictate that turbulent exchange normal to a sloping bottom must be small. As demonstrated by *Mellor* [1986] and *Mellor and Wang* [1996], the model produces bottom boundary layers with realistic properties comparable to the one-dimensional model of *Weatherly and Martin* [1978]. The penalty for this approach is that there can be vertical fluxes in the presence of vertical property gradients. The first remedy is the use of the Smagorinsky diffusivity, which is small when velocity gradients are small, as in deep water. The second remedy is to subtract climatological temperature and salinity fields from the model values before diffusion terms are calculated. In this case the model climatology tends toward the observed climatology (compared with pure horizontal diffusion, which will drive the model climatology toward horizontal homogeneity). Scale analysis shows that the relaxation timescale associated with the model diffusion is about 2 years near the surface and about 20 years in the deep ocean, compared with the Newtonian relaxation timescales of 50 days and 250 days for the surface and the deep ocean used by *Sarmiento and Bryan* [1982] and the 3 year relaxation timescale of the deep ocean used by the global model of *Semtner and Chervin* [1992]. Although the relaxation to climatology is relatively weak, it nevertheless does reduce model climate drift, as we have found in recent experiments using zero horizontal diffusion. Therefore further sensitivity studies of horizontal diffusion in sigma coordinate models are now underway.

The bottom boundary layer is important to the creation of deep water. Thus, in the Mediterranean Sea simulations of *Zavatarelli and Mellor* [1995], bottom Ekman transport is generally downslope and normal to the overriding geostrophic velocities, which are generally cyclonic and along isobaths. This process has recently received considerable attention [*Price and Baringer*, 1994;

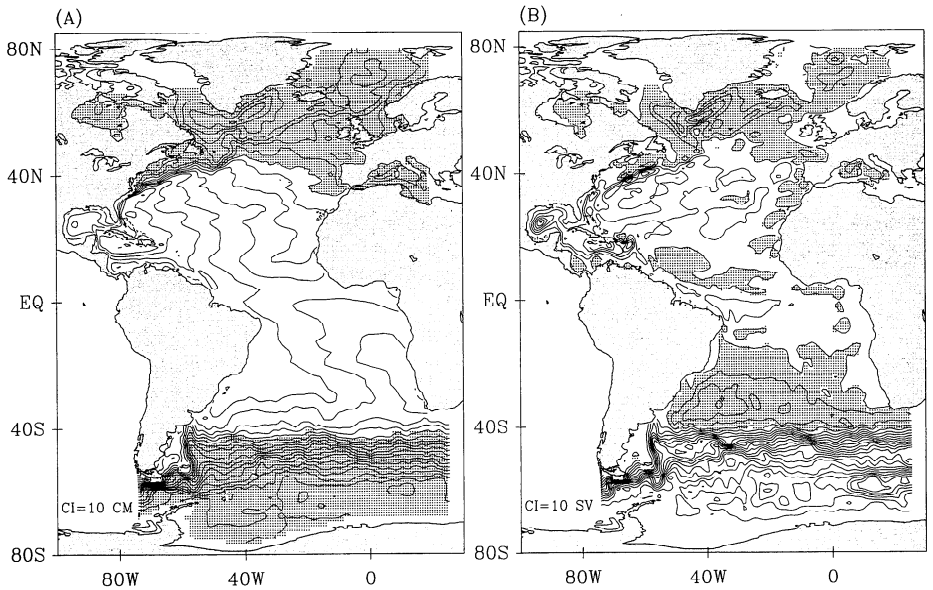

Figure 2. Five-year-averaged (years 26 to 30) model fields. (a) Surface elevation; contour interval is 10 cm. (b) Total stream function; contour interval is 10 Sv (1 Sv = 10^6 m^3 s^{-1}). Shaded areas represent negative values.

Jungclaus and Backhaus, 1994; *Jiang* and *Garwood*, 1995]. It should be noted that this downslope process is operative even if the bottom layer is crudely resolved, in which case the bottom stress determination retreats to a bulk drag coefficient formulation. In the present model the bottom layer is as thick as 500 m in the deepest water, less so on intermediate slopes. This formulation means that the downslope, Ekman transport is distributed over a thick bottom layer; nonetheless, the process is active in forming deep water, as is shown in the Mediterranean simulation. In the current model, for example, plots of bottom salinities (not shown) exhibit a coarse representation of the Mediterranean deep water tongue at the right depth, but in the future it will be important to assay the effect of improved bottom resolution. Bottom Ekman transport plays a role in the maintenance of the baroclinicity of the entire ocean water column, as shown by *Mellor and Wang* [1996]. Thus we believe that it is important to model bottom processes correctly.

3. Model Simulation Results

3.1. Horizontal Circulation and Velocities

The model was run for a 30-year period forced by monthly mean surface data as discussed above. Figure 2 shows the model climatology (a 5-year average of years 26 to 30) of the surface elevation and total stream function. Note that ocean models often produce an unrealistic Gulf Stream separation with a strong anticyclonic gyre just off Cape Hatteras [*Beckmann et al.*, 1994; *Bryan et al.*, 1995; *Dengg et al.*, 1996], but we do not see this feature here. The study of the Gulf Stream separation by *Ezer and Mellor* [1992] suggests that an important ingredient in achieving realistic separation in ocean models is to be able to resolve the northern recirculation gyre [*Mellor et al.*, 1982; *Hogg et al.*, 1986] and to maintain its water mass properties. The flow associated with the northern recirculation gyre, part of which is the topographically constrained Deep Western Boundary Current (DWBC) flowing along the continental slope, is well represented by the sigma coordinate model, as is shown later. The maximum sea level drop across the Gulf Stream is about 0.8 m, and the maximum Gulf Stream transport is about 60 Sv, both properties somewhat underestimated because of the insufficient horizontal resolution. The Gulf Stream axis inferred from surface elevation (i.e., the maximum surface velocity axis) is northward of the axis inferred from the stream function, since the latter represents the entire water column flow. The southward tilt of the deep flow with respect to the surface flow as seen in the model is consistent with observations [*Richardson*, 1985; *Hogg et al.* 1986]. Other notable features include the strong Labrador Sea circulation and the bifurcation of the ACC. Note also the surface flow from the North Atlantic into the Greenland Sea and into the Mediterranean Sea, seen in the elevation field (Figure 2a) and the 100 m velocity trajectories (Figure 3a). While the surface elevation field is quite smooth (Figure 2a), the stream function field is somewhat noisy and shows gyre structures associated with topographic variability (Figure 2b). The general circulation described by the stream function is somewhat different from the classical Sverdrup circulation or that of other z level models [e.g., *Bryan and Holland*, 1989] or isopycnal models [e.g., *Chassignet et al.*, 1996], so further discussion is in order. First, could the general circulation be the result of pressure gradient errors? Not according to *Mellor et al.* [1994], who tested this possibility by replacing the sigma coordinate calculated pressure gradient terms with terms calculated on z levels for a given density field. The results showed only very small differences in the stream function and surface elevation, as long as the procedure to minimize the errors, discussed before, is followed. Second, could the circulation be the result of artificial along-sigma diffusion? This possibility has been tested by setting the along-sigma diffusion to zero, and again the stream function did not significantly change. We therefore attribute the difference in circulation structure obtained here and obtained from z level models to the fact that the sigma coordinate model treats the density field and bottom topography (i.e., the JEBAR effect) differently from z level models. Several studies have indeed indicated the crucial role played by the JEBAR effect [*Mellor et al.*, 1982; *Greatbatch et al.*, 1991; *Ezer and Mellor*, 1994; *Ezer et al.*, 1995; *Dengg et al.*, 1996; *Myers et al.*, 1996] and show that simi-

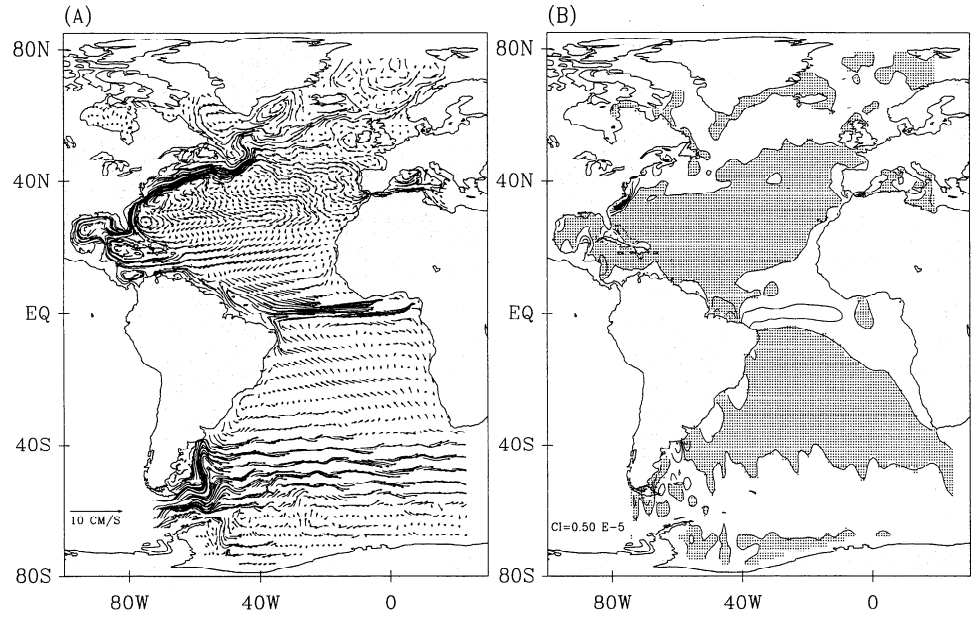

Figure 3. Five-year-averaged (years 26 to 30) velocity fields at 100 m depth. (a) Horizontal velocity trajectories (launched every second grid point) and (b) vertical velocity contour; contour interval is 0.5 x 10^{-5} m s^{-1}, and areas with negative (downward) values are shaded. The vertical velocity has been smoothed with Laplacian filter.

lar circulation patterns are found if the JEBAR effect is correctly calculated.

Figures 3, 4, and 5 show the velocity fields at 100 m, 1000 m, and near the bottom, respectively, averaged over the last 5 years of the simulation (years 26 to 30). The vertical velocity, $w(x,y,z)$, in Figures 3b, 4b and 5b can be calculated from $\omega(x,y,\sigma)$, the vertical component perpendicular to sigma layers, by using the transformation

$$w=\omega+u\left(\sigma\frac{\partial D}{\partial x}+\frac{\partial \eta}{\partial x}\right)+v\left(\sigma\frac{\partial D}{\partial y}+\frac{\partial \eta}{\partial y}\right)+\sigma\frac{\partial D}{\partial t}+\frac{\partial \eta}{\partial t}$$

where $D=H+\eta$ and where $\omega = 0$ when $\sigma = 0$ or -1. For a steady deep flow where $|\eta| << H$ a good approximation is

$$w=\omega+\sigma\left(u\frac{\partial H}{\partial x}+v\frac{\partial H}{\partial y}\right).$$

In the deepest sigma layer, ω is small so that w is dominated by the along-slope velocities. For ease of visualization the vertical fields have been smoothed with a 5-point Laplacian filter to remove small-scale noise. Trajectories, based on Eulerian velocities in Figures 3a, 4a, and 5a were launched from every second grid point.

At 100 m depth (Figure 3) the dominant features are the Gulf Stream, the eastward equatorial flow, and the Antarctic

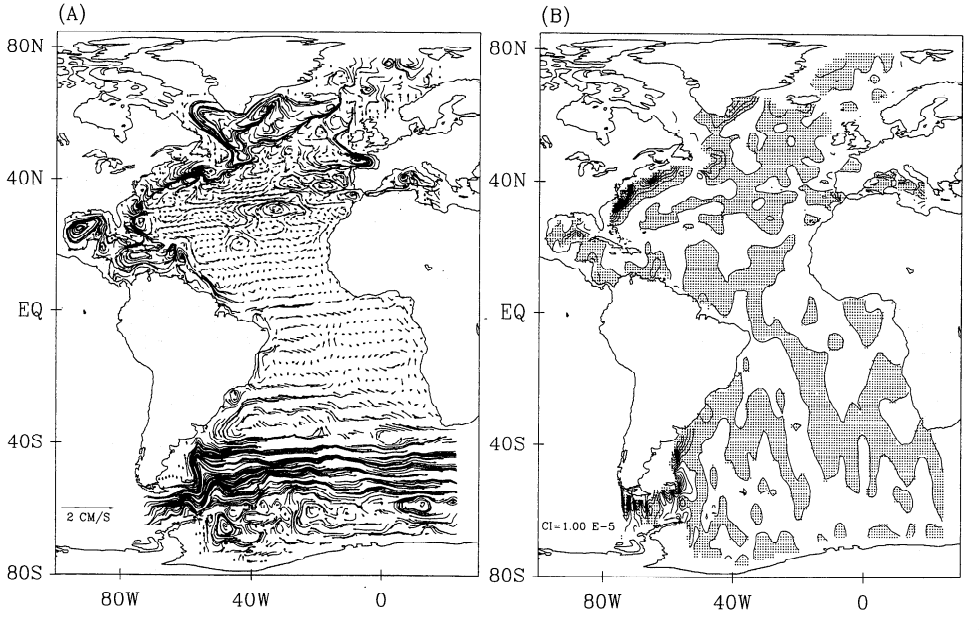

Figure 4. Same as Figure 3 but for the velocity fields at 1000 m. Contour interval in Figure 4b is 1 x 10^{-5} m s^{-1}.

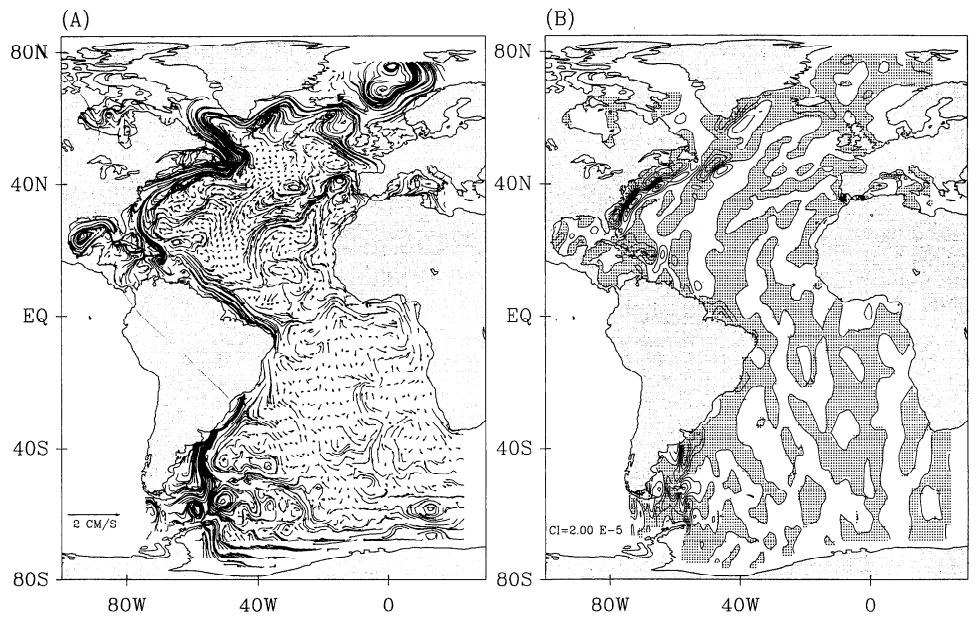

Figure 5. Same as Figure 3 but for the near-bottom sigma layer, thus velocity vectors in Figure 5a are along the bottom, and negative vertical velocities in Figure 5b represent downslope flows. Contour interval is 2×10^{-5} m s^{-1}.

Circumpolar flow. The North Atlantic Current separates into a branch that recirculates into the Labrador Sea and a branch that continues into the Greenland Sea through the Iceland-Faroe Straits. The Azores Current separates into a branch that recirculates within the subtropical gyre and a branch that continues to the European coast and into the Mediterranean Sea. The East Greenland Current, which provide Atlantic inflow through the Denmark Straits, is too weak in the model. The vertical velocity field shows the expected downward flow in middle latitudes of the North and South Atlantic resulting from the wind-driven Ekman pumping (Figure 3b). Note also the equatorial upwelling and the upwelling along the South Atlantic Bight northwest of the Gulf Stream; the latter is due to the bottom Ekman transport when the Gulf Stream flows along the continental slope before it separates from the coast at Cape Hatteras.

The horizontal flow field at 1000 m (Figure 4) shows several small-scale gyres in the North Atlantic over the mid-Atlantic Ridge and in the southern ocean south of the ACC. Note the entrainment of slope water north of the Gulf Stream into the subsurface Gulf Stream. The North Atlantic Current and the Labrador Current are evident at this depth. Areas of strong downwelling are found along western boundaries, along Greenland, the Flemish Cap, the U.S. continental slope, and the South America continental slope (Figure 4b).

In Figure 5a, near-bottom flows generally follow the bottom topography contours. The vertical component of the near-bottom flow in Figure 5b is the result of Ekman veering to the left (right) of the mean flow in the north (south) hemisphere, producing an upslope or downslope component. The DWBC is the most notable feature in the bottom flow. Note the convergence of this current along the North America continental slope (Figure 5b), with downward flow upslope of the DWBC and upward flow downslope of it. In the ACC, where horizontal resolution is finest, many gyres associated with variations in topography are found.

The regions of downslope near-bottom flow in Figure 5b (shaded areas) indicate areas of possible deep water formation. Such regions are, for example, the Mediterranean outflow, the Iceland-Faroe and the Denmark Straits, and the Labrador Sea in the North Atlantic and along the Argentinean continental shelf and the Weddell Sea in the South Atlantic.

3.2. Temperature, Salinity, and Model Climate Drift

To evaluate the model climate drift during the simulation, we examine the area-averaged vertical profiles of temperature and salinity in Figure 6. Five-year averaged model climatologies of years 6-10, 16-20 and 26-30 are compared with the initial Levitus climatology. The model climate drift is the largest during the first 5 years, with smaller drift in subsequent years. The changes in vertical structure reduce the vertical density gradients, resulting in a more diffuse model thermocline and halocline in comparison with the initial condition. While the density field in the upper 300 m or so has converged to a final state within the first 5 years, the climate drift in the deep ocean is not negligible even after 30 years in comparison with the interdecadal climate changes inferred from data [*Levitus,* 1989].

To further diagnose the climate drift of the model, the heat and salt fluxes through the open boundaries and through the surface have been calculated. Figure 7 shows, for example, the monthly averaged heat flux budget for year 26 (since climatological forcing is used, results for any other year are almost identical). Positive values represent warming trends. Lateral fluxes have been normalized by the surface area. The heat flux through the lateral open boundaries shows that the warming due to the ACC inflow in the western boundary is almost balanced by the cooling due to the ACC outflow in the east; the cooling associated with the flow between the Arctic and the Greenland Sea is small. Overall, the annual net heat flux through the lateral boundaries is equivalent to a surface warming of about 1.5 W m^{-2}. The area-averaged surface heat flux (the dashed line in Figure 7) shows a maximum summer warming comparable to the value derived from the COADS analysis (the dot-dash line in Figure 7). However, during spring and fall the model is overheated in com-

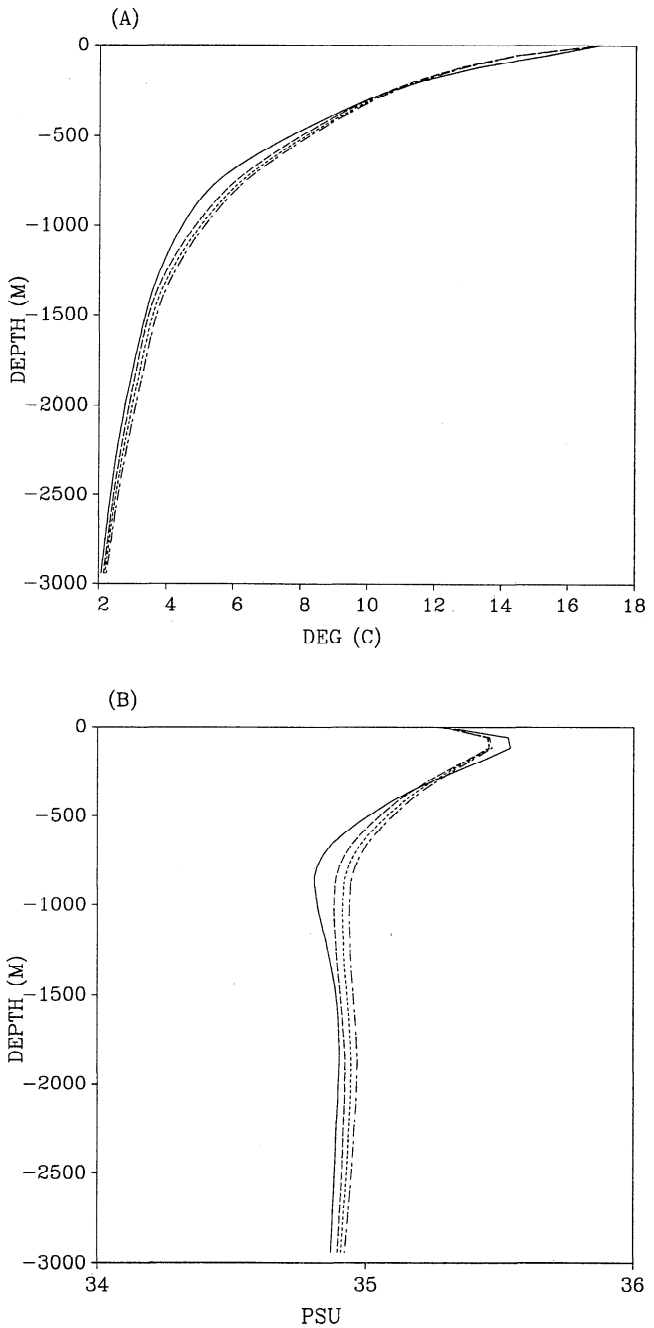

Figure 6. Vertical profiles of (a) temperatures and (b) salinities, calculated from the area averaged values over the model domain. Solid lines are for the *Levitus* [1982] annual climatology, which was used as an initial condition. Dashed, dotted, and dot-dashed lines are for the 5-year model climatologies for years 6 to 10, 16 to 20, and 26 to 30, respectively.

parison with COADS. The annual net surface heat flux in the model is about 1.8 W m^{-2}, so the total annual heat balance of the surface and lateral boundaries is about 3.3 W m^{-2}. This net heat flux causes a volume average warming trend of about 0.0065°C per year. Analysis of the model salinity budget indicates a net flux of -1 x 10^{-7} practical salinity unit (psu) m s^{-1} through the open boundaries and 3 x 10^{-7} psu m s^{-1} through the surface. The result is a trend of increasing the volume-averaged salinity by about 0.0015 psu per year. The above net heat and salinity fluxes are consistent with the climate drift shown in Figure 6.

3.3. Meridional Overturning Circulation

To simplify the presentation of the complicated three-dimensional thermohaline circulation of the ocean, a zonally averaged, meridional stream function is often calculated. Models with different grids, different mixing parameterization, different forcing, and different boundary conditions can produce quite different meridional stream functions [e.g., *Bryan and Holland*, 1989; *Semtner and Chervin*, 1992; *Delworth et al.*, 1993; *Oberhuber*, 1993; *Beckmann et al.*, 1994; *Holland and Bryan*, 1994; *Ezer and Mellor*, 1994; *Böning et al.*, 1995; *Gerdes and Koberle*, 1995; *New et al.*, 1995; *Chassignet et al.*, 1996]. Although there are no direct measurements of the thermohaline circulation, a few properties of the meridional circulation, such as the amount of deep water formation in high latitudes and the volume of the deep water transport across the equator, have been estimated from observations [e.g., *Schmitz and McCartney*, 1993; *Schmitz*, 1995] and can be compared with model results.

The model has a curvilinear orthogonal grid; to avoid interpolation errors, zonal averages are calculated along "zigzag" lines approximating each latitude (i.e., summing $u\,\Delta y$ and $v\,\Delta x$ terms if the "zigzag" line is along the model j or i lines, respectively). The total mass transports across each latitude are very small and related to the rate of change of the area-integrated elevation on either side of each latitude circle. The meridional stream function calculated from the 5-year averaged velocities for years 11-15 is shown in Figure 8a. A similar calculation for years 26-30 yields an almost identical picture, so we show only the difference between these two pentads (Figure 8b). We note, first, that interannual changes in thermohaline circulation over these 15 years are very small. The model climate drift includes some weakening of the thermohaline circulation in the middle latitudes of the North Atlantic and in the South Atlantic that do not exceed 1 Sv in most of the domain. About 8 Sv of North Atlantic Deep Water (NADW) are formed in the Greenland and the Labrador Seas

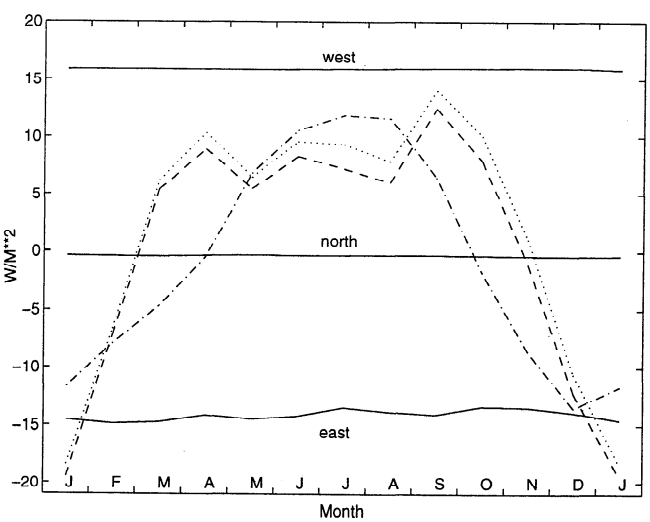

Figure 7. Monthly heat flux budget in year 26 of the model integration. Solid lines (labeled "north", "east", and "west") indicate the contribution from the three lateral open boundaries; values (in W m^{-2}) are normalized by the surface area of the model domain; positive values correspond to warming trends. The dashed and dotted lines represent the surface model heat flux and the total model heat flux (surface plus open boundaries), respectively. Also shown by the dot-dashed line is the surface monthly heat flux calculated from COADS.

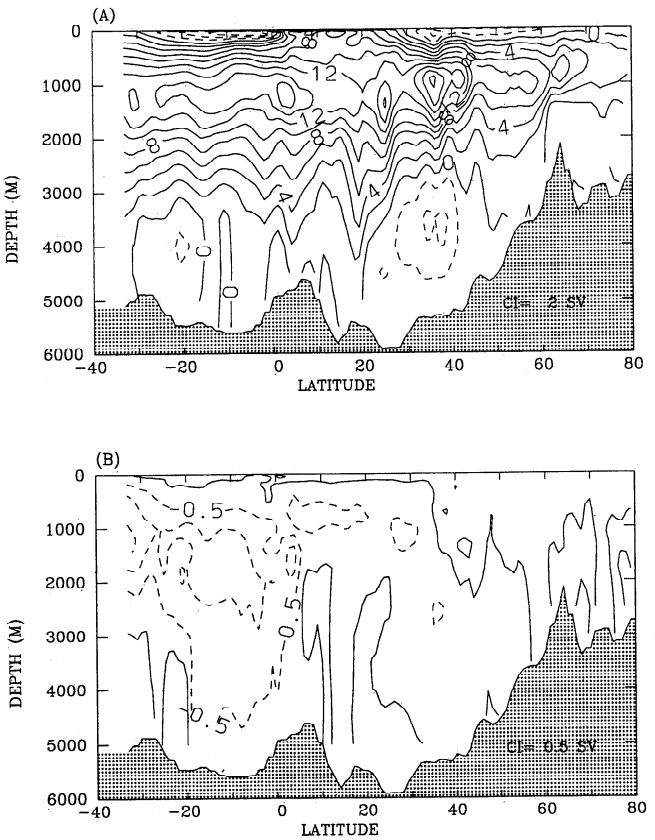

Figure 8. (a) Meridional stream function obtained from the averaged velocity fields of years 11 to 15. Contour interval is 2 Sv. (b) Meridional stream function change between the 5-year means of years 11 to 15 and years 26 to 30. Contour interval is 0.5 Sv. Negative contours (representing anticlockwise circulation) are dashed.

between 50°N and 70°N; the overflow over the sills separating the Greenland Sea and the North Atlantic can be seen in the stream function in Figure 8a around 60°N. Following the 8 Sv contour, one sees that most of this flow provides the water mass below 2000 m. An additional source of water formation in the model is found around 45°N. This cell provides water masses above 2000 m; a large part of this overturning cell recirculates and upwells in midlatitudes before it reaches the equator. The latter midlatitude overturning circulation is a new feature, which is different from the conventional picture produced, for example, by the early versions of the CME model [e.g., *Beckmann et al.*, 1994]. Because there are no direct observations of the meridional overturning circulation, we do not know whether this feature is real. Although a similar downward flow at these latitudes can also be seen in results obtained by other models, such as the global eddy resolving model of *Semtner and Chervin* [1992], the North Atlantic model of *Gerdes and Koberle* [1995] (see in particular their Figure 4b), and the isopycnal model described by *Chassignet et al.* [1996], it has not been previously discussed. The vertical flow at 1000 m and near the bottom in Figures 4b and 5b indicates that this downward flow is confined mostly to the area near the Flemish Cap, where the North Atlantic Current meets the deep portion of the Labrador Current; this finding and the results of other models mentioned above call for further investigation of the effect of local dynamics in this region with more realistic high-resolution models.

The 14-Sv of deep water flowing southward and crossing the equator is in good agreement with observational estimates [*Schmitz and McCartney*, 1993; *Schmitz*, 1995]. Some models tend to underestimate this flow [e.g., *Beckmann et al.*, 1994; *Oberhuber*, 1993; *New et al.*, 1995], either because of the close vicinity of the model southern boundary to the equator or because of artificial upwelling of the deep waters in midlatitudes as suggested by *Böning et al.* [1995] and *Chassignet et al.* [1996]; neither of these causes is a problem here. The latter two studies also show that newer versions of the CME model, which use an isopycnal mixing based on *Gent and McWilliams* [1990] instead of the standard horizontal diffusion formulation, have produced more intense overturning circulation. The deep flow in Figure 8a does not show the strong Antarctic Bottom Water (AABW) cell, compared, for example with *Beckmann et al.* [1994] or *Bryan et al.* [1995]. However, the deep flow does resemble more closely the recent results from isopycnal models and from the new versions of the CME model described by *Chassignet et al.* [1996]. The latter study suggests that the strength of the AABW cell in numerical models is directly correlated with the strength of the overturning circulation; thus our calculations are similar to other recent models that have a strong NADW cell and a very weak or nonexistent AABW cell. In any case, since the estimated observed transport associated with the AABW is only a few sverdrups [e.g., *Schmitz and McCartney*, 1993; *Schmitz*, 1995], ocean models that use a coarse vertical resolution in the deep ocean are not expected to resolve it very well. The lack of sea-ice-driven freshwater fluxes in high latitudes further limits model production of deep water masses.

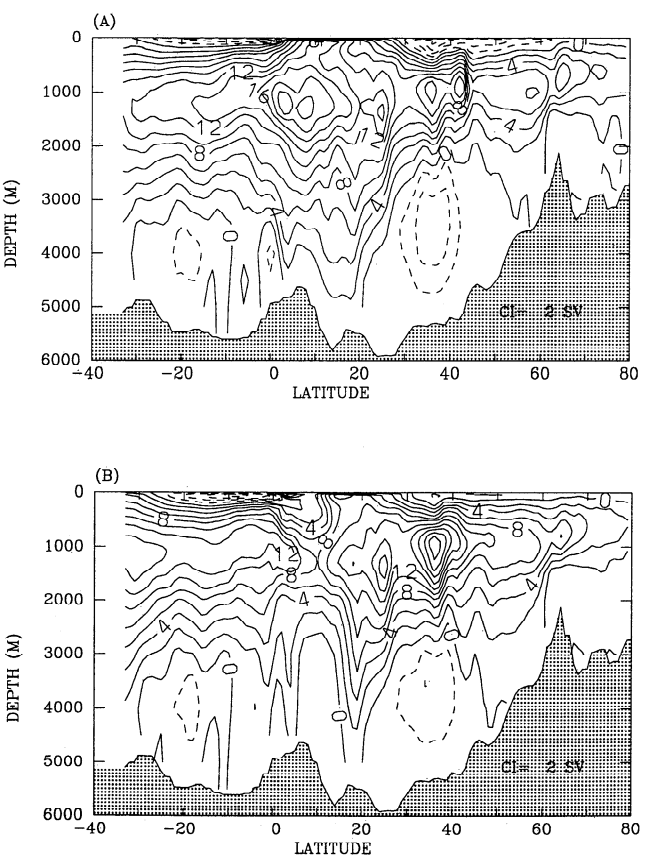

Figure 9. Same as Figure 8a, but for (a) January of year 30 and (b) July of year 30.

While interannual variations in the meridional overturning are negligible here, seasonal variations are significant (Figure 9), especially in the upper 1500 m of the ocean, though changes of a few sverdrups can be found in the equatorial deep ocean as well. These changes are associated with the seasonal changes in the winds and the corresponding changes in the Ekman transport. Weakening or strengthening of the wind-driven circulation in the upper ocean affects the opposing circulation of the deep ocean as seen in the meridional stream function; this effect has been discussed in detail by *Böning and Herrmann* [1994] and *Oberhuber* [1993] for a similar process that occurs in z level and isopycnal models. The main difference between the seasonal changes obtained here and those obtained in the CME and the isopycnal models is that the deep transport in our model is larger and thus is less affected by the upper ocean seasonal changes than are the other models mentioned.

3.4. Meridional Heat Flux

Changes in poleward meridional heat flux by the Atlantic Ocean may play an important role in changes in the climate of the ocean-atmosphere system, and thus a standard diagnostic of model calculations is the meridional heat flux. Observations with which to compare model results are usually based on analyses of atmospheric fluxes [*Isemer et al.*, 1989; *da Silva et al.*, 1994] or direct oceanic measurements, usually taken at one zonal cross section [*Hall and Bryden*, 1982; *Molinari et al.*, 1990; *Lee et al.*, 1990; *Fillenbaum et al.*, 1997]. These observations estimate the maximum meridional heat flux in the subtropical North Atlantic to be a value between 1 and 1.7 PW (1 PW = 10^{15} W). While several ocean models with different resolutions tend to underestimate the maximum meridional heat flux [*Bryan and Holland*, 1989; *Beckmann et al.*, 1994; *New et al.*, 1995], other models, such as the Miami Isopycnal Coordinate Ocean Model and new versions of the CME model with isopycnal diffusion, do produce larger values, closer to the observed estimates [*Böning et al.*, 1995; *Chassignet et al.*, 1996] and closer to our calculations.

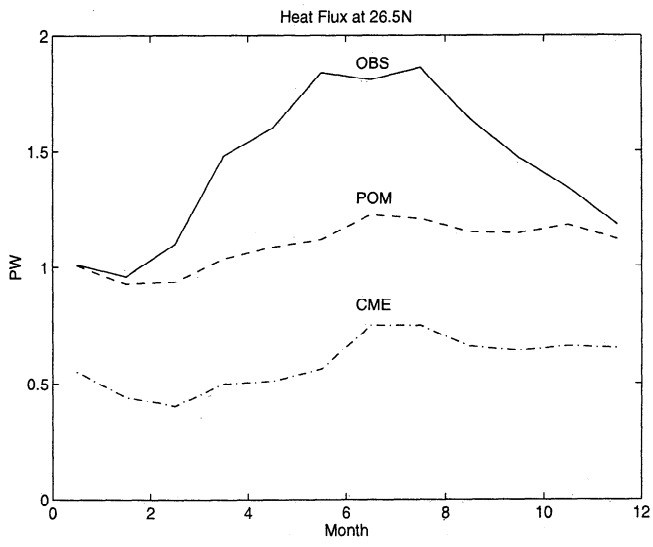

Figure 11. Meridional heat flux across 26.5°N. The solid and the dot-dashed lines represent an estimate based on observations and results from 5-year run of the Community Modeling Efforts (CME) model, respectively (as shown by *Fillenbaum et al.* [1997]). The dashed line represents results from the current simulation of the Princeton Ocean Model (POM).

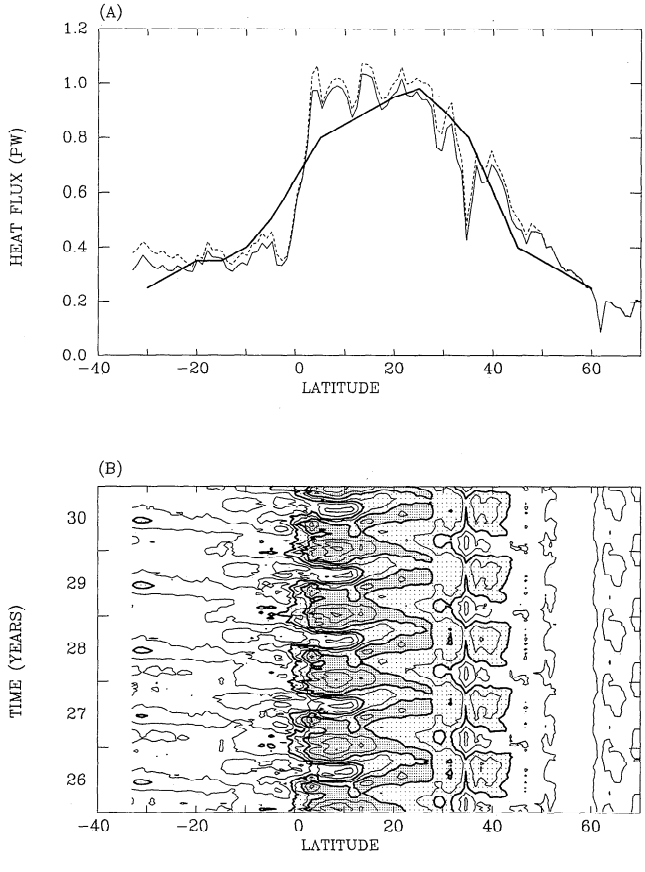

Figure 10. Zonally averaged, northward meridional heat flux. (a) Time-averaged heat flux as a function of latitude obtained from the COADS data [*da Silva et al.*, 1994] (bold solid line), the model mean climatology of years 11 to 15 (dotted line), and the model mean climatology of years 26 to 30 (light solid line). (b) Variations in meridional heat flux as a function of latitude and time for years 26 to 30. The contour interval is 0.2 PW; the light shaded areas indicate values between 0.6 and 1 PW, and the darker shaded areas indicate values larger than 1 PW.

Figure 10a shows the model meridional heat flux calculated from 5-year averaged fields for years 11-15 and 26-30. Also shown is the heat flux calculated by *da Silva et al.* [1994] using the COADS data. The general agreement between the model and the observations is quite good. However, the model with its higher resolution compared with the smooth COADS data shows more spatial variations and higher values in the subtropical North Atlantic. During the 15-year intervening period the heat flux decreases by less than 0.1 PW, a small climate drift due to the weakening of the thermohaline circulation (Figure 8b), but comparable to estimates of real climate changes over a 15-year period [*Ezer et al.*, 1995].

Figure 10b shows the temporal and spatial variations in meridional heat flux during the last 5 years of the integration. The variations are dominated by seasonal changes, with the maximum heat flux, larger than 1 PW (the dark shaded area), moving between 5°N in the winter to 25°N in the summer. Note that while the model of *Böning and Herrmann* [1994] shows negative (i.e., southward heat flux) near the equator during winter, here heat flux is northward all year long. Although some studies indicate a southward winter heat flux [e.g., *Lamb and Bunker*, 1982], more recent long-term observations [*Molinari et al.*, 1990; *Lee et al.*, 1990; *Fillenbaum et al.*, 1997] suggest that those findings were not correct because of inaccuracies in atmospheric data and that

subtropical heat flux is positive all year long, in agreement with our results. A maximum seasonal change of about 1.5 PW is found around 10°N, driven by the seasonal change of winds over the subtropical ocean; see for example, *Böning and Herrmann* [1994] for more detail. An additional secondary maximum around 40°N, not shown by *Böning and Herrmann* [1994], relates to the overturning cell around this latitude, as can be seen in Figure 9. In the model this cell changes its strength seasonally; during wintertime, when the eastward wind component strengthens, larger southward Ekman transport in the upper layers tends to decrease the strength of this cell (Figure 9a) and reduce the northward heat flux there. The maximum seasonal variations in the model are obtained around 10°N; they are comparable to those measured by *Molinari et al.* [1990] and *Lee et al.* [1990] at 26.5°N and displayed in Figure 11. Also displayed in Figure 11 is a comparison with calculations of the CME model, which uses standard horizontal diffusion; see *Fillenbaum et al.* [1997] for detail comparison between observations and the CME results. The observed estimate at 26.5°N is based on observations of the Florida current taken during 1982-1984 [*Molinari et al.*, 1990], mooring array data off Abaco during 1987-1992 [*Fillenbaum et al.*, 1997], and the Levitus monthly climatology and wind-driven Ekman transport to estimate the interior heat flux. While the model annual mean heat flux at 26.5°N is quite realistic, the annual cycle is underestimated in both POM and CME models. The discrepancy between the models and the observations is partly due to the climatological wind data used in the models. In addition, likely errors in the observed estimates are due to the interior heat flux estimates, which are not directly observed, and errors due to mesoscale and interannual variations.

4. Discussion and Conclusions

In preparation for a study of Atlantic Ocean climate change a 30-year-long climatological simulation has been performed. Since this is the first time that this sigma coordinate model has been applied to the entire Atlantic Ocean, the basic circulation features obtained by the model have been presented and compared with observations and with other models such as z level and isopycnal models. The results clearly indicate many differences between the different models; not all of them can be fully understood, since the models not only differ algorithmically, but also have different surface forcing, boundary conditions, mixing parameterization, and resolution. The main difference between this model and the more conventional z level models is the way bottom topography is treated in the sigma coordinate model and the parameterization of horizontal diffusion. The horizontal circulation, which consists of deep flow gyres and recirculations, is quite different from the classical picture given by the Sverdrup circulation or previous coarse resolution models but resembles the results of models that explicitly calculate the topographical effects associated with the JEBAR term [*Mellor et al.*, 1982; *Greatbatch et al.*, 1991; *Myers et al.*, 1996]. Since the continental slope and the continental shelf are included in the calculations, possible artificial effects associated with sea-land boundaries, which are represented in z level models by vertical walls, are removed. The representation of the JEBAR term in the sigma coordinate model could be the reason Gulf Stream separation and its associated recirculations (Figure 2b) are produced quite well here, considering the modest resolution. The notion that the representation of the JEBAR term in ocean models is crucial in determining the Gulf Stream separation has been supported by the recent studies of *Dengg et al.* [1996] and *Myers et al.* [1996]. The above discussion applies also to the thermohaline overturning circulation structure, which is also different from some of the previous simulations with z level models such as the CME. It is interesting to note, however, that sensitivity studies with the CME model by *Holland and Bryan* [1994] show that when the above standard model [see *Bryan and Holland*, 1989] is modified to be closer to our POM configuration, i.e., with open boundary conditions and reduced diapycnal mixing, the results resemble our calculations much more closely than do the standard CME calculations. For example, meridional heat flux increases to more realistic values, the intensity of the NADW cell increases, the intensity of the AABW cell decreases, and a signature of the downward flow around 45°N emerges.

Acknowledgments. The research was supported by NOAA's Atlantic Climate Change Program, grant NA36GP0262, by the Office for Naval Research grant N00014-93-1-0037; by NOAA's Coastal Ocean Program; and by the computational support and facilities of NOAA's Geophysical Fluid Dynamics Laboratory.

References

Beckmann, A., C. W. Böning, C. Koberle, and J. Willebrand, Effects of increased horizontal resolution in a simulation of the North Atlantic ocean, *J. Phys. Oceanogr., 24*, 326-344, 1994.

Blumberg, A. F., and G. L. Mellor, A description of a three-dimensional coastal ocean circulation model, in *Three-Dimensional Coastal ocean Models*, *Coastal Estuarine Ser.*, vol. 4, edited by N. S. Heaps. 208 pp., AGU, Washington, D. C., 1987.

Böning, C. W., and P. Herrmann, Annual cycle of poleward heat transport in the ocean: Results from high-resolution modeling of the North and equatorial Atlantic, *J. Phys. Oceanogr., 24*, 91-107, 1994.

Böning, C. W., W. R. Holland, F. O. Bryan, G. Danabasoglu, and J. McWilliams, An overlooked problem in model simulation of the thermohaline circulation and heat transport in the Atlantic Ocean, *J. Clim., 8*, 514-523, 1995.

Bryan, F. O., and W. R. Holland, A high-resolution simulation of the wind and thermohaline-driven circulation of the North Atlantic Ocean, in *Contribution to 'Aha Huliko'a, The Proceedings of the Hawaiian Winter Workshop*, pp. 99-116, University of Hawaii, Hololulu, 1989.

Bryan, F. O., C. W. Böning, and W. R. Holland, On the midlatitude circulation in a high-resolution model of the North Atlantic, *J. Phys. Oceanogr., 25*, 289-305, 1995.

Chassignet, E. P., L. T. Smith, R. Bleck, and F. O. Bryan, A model comparison: Numerical simulations of the North and equatorial Atlantic circulation in depth and isopycnic coordinates, *J. Phys. Oceanogr., 26*, 1849-1867, 1996.

da Silva, A. M., C. C. Young, and S. Levitus, *Atlas of Surface Marine Data 1994*, vol. 3, *Anomalies of Heat and Momentum Fluxes*, *NOAA Atlas NESDIS 8*, 413 pp., Natl. Env. Sat. Data Inf. Serv., Washington, D. C., 1994.

Delworth, T., S. Manabe, and R. J. Stouffer, Interdecadal variations of the thermohaline circulation in a coupled ocean-atmosphere model, *J. Clim., 6*, 1993-2011, 1993.

Dengg, J., A. Beckmann, and R. Gerdes, The Gulf Stream separation problem, in *The Warmwatersphere of the North Atlantic Ocean*, edited by W. Krauss, pp. 253-290, Gebrüder Borntraeger, Berlin, 1996.

Ezer, T., and G. L. Mellor, A numerical study of the variability and the separation of the Gulf Stream induced by surface atmospheric forcing and lateral boundary flows, *J. Phys. Oceanogr., 22*, 660-682, 1992.

Ezer, T., and G. L. Mellor, Diagnostic and prognostic calculations of the North Atlantic circulation and sea level using a sigma coordinate ocean model, *J. Geophys. Res., 99*, 14,159-14,171, 1994.

Ezer, T., G. L. Mellor, and R. J. Greatbatch, On the interpentadal variability of the North Atlantic ocean: Model simulated changes in transport, meridional heat flux and coastal sea level between 1955-1959 and 1970-1974, *J. Geophys. Res., 100*, 10,559-10,566, 1995.

Fillenbaum, E. R., T. N. Lee, W. E. Johns, and R. J. Zantopp, Meridional heat transport variability at 26.5°N in the North Atlantic, *J. Phys. Oceanogr., 27*, 153-174, 1997.

Fujio, S., T. Kadowaki, and N. Imasato, World ocean circulation diagnostically derived from hydrographic and wind stress fields, 1, The velocity field, *J. Geophys. Res.*, *97*, 11,163-11,176, 1992.

Gent, P. R., and J. C. McWilliams, Isopycnal mixing in ocean circulation models, *J. Phys. Oceanogr.*, *20*, 150-155, 1990.

Gerdes, R., A primitive equation ocean circulation model using a general vertical coordinate transformation, 1, Description and testing of the model, *J. Geophys. Res.*, *98*, 14,683-14,701, 1993.

Gerdes, R., and C. Koberle, On the influence of DSOW in numerical model of the North Atlantic general circulation, *J. Phys. Oceanogr.*, *25*, 2624-2642, 1995.

Greatbatch, R. J., A. F. Fanning, A. D. Goulding, and S. Levitus, A diagnosis of interpentadal circulation changes in the North Atlantic, *J. Geophys. Res.*, *96*, 22,009-22,023, 1991.

Greatbatch, R. J., G. Li, and S. Zhang, Hindcasting ocean climate variability using time-dependent surface data to drive a model: An idealized study, *J. Phys. Oceanogr.*, *25*, 2715-2725, 1995.

Haidvogel, D. B., and A. Beckmann, Numerical modeling of the coastal ocean, in *The Sea*, John Wiley, New York, in press, 1997.

Häkkinen, S., and G. L. Mellor, Modeling the seasonal variability of a coupled Arctic ice-ocean system, *J. Geophys. Res.*, *97*, 20,285-20,304, 1992.

Hall, M. M., and H. L. Bryden, Direct estimates and mechanisms of ocean heat transport, *Deep Sea Res.*, *29*, 339-359, 1982.

Haney, R. L., On the pressure gradient force over steep topography in sigma coordinate ocean models, *J. Phys. Oceanogr.*, *21*, 610-619, 1991.

Hecht, M. W., W. R. Holland, V. Artale, and N. Pinardi, North Atlantic model sensitivity to Mediterranean waters, in *Assessing Climate Change: Results from the Model Evaluation Consortium for Climate Assessment*, edited by W. Howe and A. Henderson-Sellers, Gordon and Breach, Newark, N. J., in press, 1997.

Hogg, N. G., R. S. Pickart, R. M. Hendry, and W. J. Smethie, The northern recirculation gyre of the Gulf Stream, *Deep Sea Res.*, *33*, 1139-1165, 1986.

Holland, W. R., and F. O. Bryan, Sensitivity studies on the role of the ocean in climate change, *Ocean Processes in Climate Dynamics: Global and Mediterranean Examples*, edited by P. Malanotte-Rizzoli and A. R. Robinson, pp. 111-134, Kluwer, Dordrecht, The Netherlands, 1994.

Isemer, H. J., J. Willebrand, and L. Hasse, Fine adjustment of large scale air-sea energy flux parameterization by a direct estimate of ocean heat transport, *J. Clim.*, 2, 1173-1184, 1989.

Jiang, L., and R. W. Garwood Jr., A numerical study of three-dimensional dense bottom plumes on a Southern Ocean continental slope, *J. Geophys. Res.*, *100*, 18,471-18,488, 1995.

Jungclaus, J. H., and J. O. Backhaus, Application of a transient reduced gravity plume model to the Denmark Strait Overflow, *J. Geophys. Res.*, *99*, 12,375-12,396, 1994.

Lamb, P. J., and A. F. Bunker, The annual march of the heat budget of the north and tropical Atlantic Oceans, *J. Phys. Oceanogr.*, *12*, 1388-1409, 1982.

Lee, T. N., W. E. Johns, F. Schott, and R. Zantopp, Western boundary current structure and variability east of Abaco, Bahamas, at 26.5°N, *J. Phys. Oceanogr.*, *20*, 446-466, 1990.

Levitus, S., Climatological atlas of the world ocean, *NOAA Prof. Pap.*, *13*, 173 pp., Natl. Oceanic and Atmos. Admin., Washington, D. C., 1982.

Levitus, S., Interpentadal variability of temperature and salinity in the deep North Atlantic, 1970-1974 versus 1955-1959, *J. Geophys. Res.*, *94*, 16,125-16,131, 1989.

Mellor, G. L., Numerical simulation and analysis of the mean coastal circulation off California, *Cont. Shelf Res.*, *6*, 689-713, 1986.

Mellor, G. L., User's guide for a three-dimensional, primitive equation, numerical ocean model, 40 pp., Program in Atmos. and Ocean. Sci. report, Princeton Univ., Princeton, N. J., 1996.

Mellor, G. L., and A. F. Blumberg, Modeling vertical and horizontal diffusivities with the sigma coordinate system, *Mon. Weather Rev.*, *113*, 1380-1383, 1985.

Mellor, G. L., and T. Ezer, Sea level variations induced by heating and cooling: An evaluation of the Boussinesq approximation in ocean model, *J. Geophys. Res.*, *100*, 20,565-20,577, 1995.

Mellor, G. L., and X. H. Wang, Pressure compensation and the bottom boundary layer, *J. Phys. Oceanogr.*, *26*, 2214-2222, 1996.

Mellor, G. L., and T. Yamada, Development of a turbulence closure model for geophysical fluid problems. *Rev. Geophys.*, *20*, 851-875, 1982.

Mellor, G. L., C. Mechoso, and E. Keto, A diagnostic calculation of the general circulation of the Atlantic Ocean, *Deep Sea Res.*, *29*, 1171-1192, 1982.

Mellor, G. L., T. Ezer, and L. Y. Oey, The pressure gradient conundrum of sigma coordinate ocean models, *J. Atmos. Oceanic Technol.*, *11*, 1126-1134, 1994.

Molinari, R. L., E. Johns, and J. Festa, The annual cycle of meridional heat flux in the Atlantic Ocean at 26.5°N, *J. Phys. Oceanogr.*, *20*, 476-482, 1990.

Myers, P. G., A. F. Fanning, and A. J. Weaver, JEBAR, bottom pressure torque, and Gulf Stream separation, *J. Phys. Oceanogr.*, *26*, 671-683, 1996.

New, A. L., R. Bleck, Y. Tia, R. Marsh, M. Huddleston, and S. Barnard, An isopycnic model study of the North Atlantic, I, Model experiment, *J. Phys. Oceanogr.*, *25*, 2667-2699, 1995.

Oberhuber, J. M., Simulation of the Atlantic circulation with a coupled sea ice-mixed layer-isopycnal general circulation model, II, Model experiment, *J. Phys. Oceanogr.*, *23*, 830-845, 1993.

Pacanowski, R., K. Dixon, and A. Rosati, The G.F.D.L. Modular Ocean Model user's guide, *GFDL Ocean Group Tech. Rep. 2*, 44 pp., Geophys. Fluid Dyn. Lab., Princeton, N. J., 1991.

Price, J. F., and M. O. Baringer, Outflow and deep water production by marginal seas, *Prog. Oceanogr.*, *33*, 161-200, 1994.

Richardson, P. L., Average velocity and transport of the Gulf Stream near 55 W, *J. Mar. Res.*, *43*, 83-111, 1985.

Sarmiento, J. L., and K. Bryan, An ocean transport model for the North Atlantic, *J. Geophys. Res.*, *87*, 394-408, 1982.

Schmitz, W. J., On the interbasin-scale thermohaline circulation, *Rev. Geophys.*, *33*, 151-173, 1995.

Schmitz, W. J., and M. S. McCartney, On the North Atlantic circulation, *Rev. Geophys.*, *31*, 29-49, 1993.

Semtner, A. J., and R. M. Chervin, Ocean general circulation from a global eddy-resolving model, *J. Geophys. Res.*, *97*, 5493-5550, 1992.

Smagorinsky, J., S. Manabe, and J. L. Holloway, Numerical results from a nine-level general circulation model of the atmosphere, *Mon. Weather Rev.*, *93*, 727-768, 1965.

Tziperman, E., R. Toggweiler, Y. Felix, and K. Bryan, Instability of the thermohaline circulation with respect to mixed boundary conditions: Is it really a problem for realistic models?, *J. Phys. Oceanogr.*, *24*, 217-232, 1994.

Weatherly, G. L., and P. J. Martin, On the structure and dynamics of the oceanic bottom boundary layer, *J. Phys. Oceanogr.*, *8*, 557-570, 1978.

Weaver, A. J., E. S. Sarachik, and J. Marotzke, Freshwater flux forcing of decadal and interdecadal oceanic variabilities, *Nature*, *353*, 836-838, 1991.

Whitworth, T., and R. G. Peterson, Volume transport of the Antarctic Circumpolar Current from bottom pressure measurements, *J. Phys. Oceanogr.*, *15*, 810-816, 1985.

Willems, R. C., S. M. Glenn, M. F. Crowley, P. Malanotte-Rizzoli, R. E. Young, T. Ezer, G. L. Mellor, H. G. Arango, A. R. Robinson, and C.-C. A. Lai, Experiment evaluates ocean models and data assimilation in the Gulf Stream, *Eos, Trans., AGU*, *75*, 385-394, 1994.

Zavatarelli, M., and G. L. Mellor, A numerical study of the Mediterranean Sea circulation, *J. Phys. Oceanogr.*, *25*, 1384-1414, 1995.

T. Ezer and G. L. Mellor, Program in Atmospheric and Oceanic Sciences, P.O. Box CN710, Sayre Hall, Princeton University, Princeton, NJ 08544-0710. (e-mail: ezer@splash.princeton.edu)

(Received October 10, 1996; revised March 17, 1997;
accepted March 31, 1997.)